Effective temporal resolution in pump-probe spectroscopy with strongly chirped pulses

D. Polli,[1,2,*] D. Brida,[1] S. Mukamel,[3] G. Lanzani,[1,2] and G. Cerullo[1]

[1]*IFN-CNR, Dipartimento di Fisica, Politecnico di Milano, Piazza Leonardo da Vinci 32, I-20133 Milano, Italy*

[2]*CNST, Istituto Italiano di Tecnologia, Dipartimento di Fisica, Politecnico di Milano, Piazza Leonardo da Vinci 32, I-20133 Milano, Italy*

[3]*Chemistry Department, University of California, Irvine, Irvine, California 92697-2025, USA*

(Received 24 July 2009; revised manuscript received 1 June 2010; published 11 November 2010)

This paper introduces a general theoretical description of femtosecond pump-probe spectroscopy with chirped pulses whose joint spectral and temporal profile is expressed by Wigner spectrograms. We demonstrate that the actual experimental time resolution intimately depends on the pulse-sample interaction and that the commonly used instrumental response function needs to be replaced by a sample-dependent effective response function. We also show that, using the proper configurations in excitation and/or detection, it is possible to overcome the temporal smearing of the measured dynamics due to chirp-induced pulse broadening and recover the temporal resolution that would be afforded by the transform-limited pulses. We verify these predictions with experiments using broadband chirped pump and probe pulses. Our results allow optimization of the temporal resolution in the common case when the chirp of the pump and/or probe pulse is not corrected and may be extended to a broad range of time-resolved experiments.

DOI: 10.1103/PhysRevA.82.053809 PACS number(s): 42.65.Re, 78.47.J−, 82.53.Kp

I. INTRODUCTION

Femtosecond pump-probe spectroscopy is the most powerful and commonly used experimental technique for the study of primary photoinduced dynamical processes in physics, chemistry, and biology [1,2]. The need to excite optical transitions in resonance and detect spectral signatures of transient states manifesting themselves at different frequencies calls for broad tunability of pump and probe pulses, from the ultraviolet to the midinfrared spectral range [3]. With the goal of improving the temporal resolution, a great effort has been devoted to the generation of ultrabroadband light pulses and to their compression to the transform-limited (TL) duration, down to just a few cycles of the carrier wavelength [4]. However, the precise control of the relative timing of the various frequency components of ultrabroadband pulses is extremely challenging, especially in frequency ranges where material dispersion is strong or where dispersive delay lines are not readily available. The frequency chirp can extend the duration of pump and probe pulses way beyond the TL values and thus degrade the temporal resolution of the technique, preventing the observation of fast dynamics. It is therefore very important, for a variety of experiments, to evaluate the temporal resolution of pump-probe spectroscopy with chirped pulses, as a function of excitation and detection conditions.

In experiments with relatively narrow-band (>100-fs-duration) TL pulses, the time resolution is commonly assumed to be the width of the instrumental response function, which is defined as the cross-correlation between the temporal intensity profiles of pump and probe pulses [5]. This simple criterion breaks down for broadband pulses and the effective time resolution becomes more subtle [6–9]. The white-light continuum (WLC) generated in a bulk material (such as sapphire) is a common tool for broadband pump-probe spectroscopy but often has a strong frequency chirp [10]. Kovalenko *et al.* demonstrated that for a chirped WLC probe pulse [7], it is possible to account for the wavelength-dependent zero timing and that the time-corrected transient signal, when measured with chirped probe pulses, is given by the same expression as that obtained with nonchirped pulses. The role of the pump chirp is more intriguing. It has been shown that a negative/positive chirp in ultrabroadband pump pulses enhances/reduces the relative weight of ground-state and excited-state coherent oscillations [11–14], and chirped midinfrared pulses have been used for vibrational ladder climbing [15,16].

In this paper we develop a precise and general definition of the effective temporal resolution achievable with chirped pulses and its variation with both excitation and detection conditions. We accomplish this goal using Wigner spectrograms (WSs), which provide the joint spectral and temporal description of the pulses. We show that the actual time resolution of the experiment depends on the pulse-sample interaction and that the instrumental response function needs to be replaced by a sample-dependent *effective* response function (ERF). We also demonstrate that, using the proper configurations in excitation and/or detection, it is possible to overcome the temporal smearing of the measured dynamics due to the chirp-induced pulse broadening and to recover the temporal resolution that would be afforded by the TL pulses. We verify these predictions with experiments using broadband chirped pump and probe pulses. Our results can be applied to a broad range of time-resolved experiments and allow optimization of the temporal resolution in the common case when the chirp of the pump and/or probe pulse is not corrected.

This paper is organized as follows. In Sec. II we first recall the definition of the WS and its use for describing the time-frequency structure of chirped pulses. Using the third-order perturbative formalism for nonlinear spectroscopy, we express the pump-probe signal in terms of the WS of the pump and the probe pulses. We introduce two functions, which we call preparation and observation windows, to describe the interactions of pump and probe pulses with the sample

*dario.polli@polimi.it

and the measurement apparatus, respectively. We then show that the time resolution with chirped pulses is determined by an ERF which is the cross-correlation between the two windows. In Sec. III we first introduce our experimental setup for broadband pump-probe spectroscopy with chirped pulses, and we then report experimental results which support the theoretical analysis. Finally, in Sec. IV we draw our conclusions and discuss possible future applications of our results.

II. DERIVATION OF THE TIME- AND FREQUENCY-DEPENDENT PUMP-PROBE SIGNAL WITH CHIRPED PULSES

A. The Wigner spectrogram

The WS is a two-dimensional depiction of the joint time and frequency profile of a pulse, which allows one to represent the pulse chirp in a very intuitive way by revealing the temporal distribution of its different spectral components [17,18]. The WS for the complex electric field $E(t)$ of an optical pulse is defined as

$$W(\omega,t) = \int_{-\infty}^{\infty} E^*\left(t - \frac{\tau}{2}\right) E\left(t + \frac{\tau}{2}\right) e^{i\omega\tau} d\tau \qquad (1a)$$

or, alternatively, as a frequency-domain integral,

$$W(\omega,t) = \int_{-\infty}^{\infty} \tilde{E}^*\left(\omega - \frac{\Omega}{2}\right) \tilde{E}\left(\omega + \frac{\Omega}{2}\right) e^{-i\Omega t} d\Omega, \quad (1b)$$

where $\tilde{E}(\omega) = \int_{-\infty}^{+\infty} E(t) e^{i\omega t} dt$ is the Fourier transform of the field $E(t)$. The WS allows one to visualize the fraction of field energy which is contained in a given time and frequency window of the pulse. The temporal marginal of the WS (i.e., its integral over frequency) gives the pulse temporal intensity profile,

$$2|E(t)|^2 = \int_{-\infty}^{+\infty} W(\omega,t)\, d\omega, \qquad (2a)$$

while the frequency marginal of the WS (i.e., its integral over time) gives the energy spectral density of the pulse,

$$|\tilde{E}(\omega)|^2 = \int_{-\infty}^{+\infty} W(\omega,t)\, dt. \qquad (2b)$$

As an example, Figs. 1(a) and 1(b) show the WS for TL Gaussian pulses at a 375-THz carrier frequency (800-nm wavelength) with 100- and 10-fs FWHM durations, respectively. Figures 1(d) and 1(e) depict the corresponding temporal intensity profiles (i.e., the temporal marginals of the WS). Figure 1(c) shows the WS for the pulse in Fig. 1(b) with a strong frequency chirp (with a purely quadratic spectral phase), which causes a broadening of the temporal intensity profile up to a duration of 100 fs [see solid(red) line in Fig. 1(f)]. The narrow and elongated shape of the WS for the chirped pulse is caused by a temporal shearing of the WS of the corresponding TL pulse, as the various frequency components of the pulse occur at different times. It is important to note that, while the temporal intensity profile of the chirped pulse is dramatically broadened, any horizontal cut of the WS at a given frequency

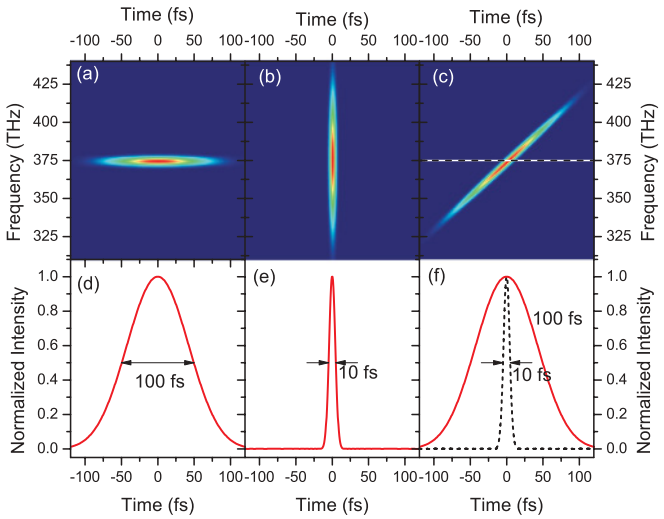

FIG. 1. (Color online) (a–c) WSs of three pulses with a 375-THz carrier frequency: two TL Gaussian pulses, 100 fs (a) and 10 fs (b) in duration, and a strongly chirped pulse with a pure quadratic phase (GDD = 360 fs^2), causing a temporal broadening up to a spectrally integrated duration of 100 fs (c). (d–f) Temporal profiles obtained by spectrally slicing the three pulses at their center frequency; the dashed line in (f) represents the corresponding spectrally -integrated pulse temporal profile.

preserves the duration of the TL pulse. This is rigorously true for a pulse with a quadratic spectral phase:

$$\tilde{E}_{\mathrm{CHIRPED}}(\omega) = \tilde{E}_{\mathrm{TL}}(\omega)\exp[iD\omega^2/2], \qquad (3)$$

where $\tilde{E}_{\mathrm{TL}}(\omega)$is the TL pulse spectrum and D is the group delay dispersion (GDD). It can be shown using Eq. (1b) that its WS is

$$W_{\mathrm{CHIRPED}}(\omega,t) = W_{\mathrm{TL}}(\omega, t - D\omega), \qquad (4)$$

where W_{TL} is the WS of the TL pulse. Therefore, any spectral slice of the WS of such a chirped pulse at a given frequency [see dashed (black) lines in Fig. 1(f)] is simply a rigid temporal translation of the corresponding slice for a TL pulse, thus causing the W_{CHIRPED} to be a sheared replica of the W_{TL}. In the presence of significant higher-order dispersion (cubic etc.), W_{CHIRPED} is not a simple sheared replica of the W_{TL}, but in general the distortions are limited (see Sec. III A).

B. Pump-probe spectroscopy with chirped pulses

The signal for a general $\chi^{(3)}$ nonlinear spectroscopy can be written by the following nested-integral expression [2]:

$$I_{\mathrm{pp}} = \int_{-\infty}^{\infty} d\tau_4 \int_{-\infty}^{\tau_4} d\tau_3 \int_{-\infty}^{\tau_3} d\tau_2 \int_{-\infty}^{\tau_2} d\tau_1 E_4(\tau_4) \times E_3(\tau_3) E_2(\tau_2) E_1(\tau_1) S(\tau_1,\tau_2,\tau_3,\tau_4), \qquad (5)$$

where the sample response S is a function of the four time axes τ_1–τ_4 of the electric fields E_1–E_4 of the four optical pulses [19].

Pump-probe spectroscopy is a self-heterodyning technique where only two optical pulses are used for studying the ultrafast

dynamics of the sample. The first pulse reaching the sample is called the *pump* $[E_{pu}(t)]$ and acts as a nearly impulsive perturbation, while the second pulse [called the *probe;* $E_{pr}(t)$] investigates the sample evolution at different delays with respect to the pump. In this case, each pulse contributes twice to the interacting fields. If we consider temporally well-separated pump and probe pulses [20,21], we can perform the integration independently on each contribution, so that the pump-probe signal I_{pp} can be written as

$$I_{pp} = \int_{-\infty}^{\infty} dt'' \int_{-\infty}^{t''} d\tau'' \int_{-\infty}^{\infty} dt' \int_{-\infty}^{t'} d\tau' E_{pr}^{*}(t'') \times E_{pr}(\tau'') S(t'',\tau'',t',\tau') E_{pu}^{*}(t') E_{pu}(\tau'). \quad (6)$$

It should be noted that time ordering between the two pump/probe fields, $E_j^*(t)$ and $E_j(\tau)$, is lost so that all integrals can be extended from $-\infty$ to ∞.

By some simple mathematical manipulations, which are reported in the Appendix, the pump-probe signal can be expressed in terms of the WS of pump and probe pulses, obtaining

$$I_{pp} = \frac{1}{(2\pi)^2} \int d\omega_{pr} \int d\omega_{pu} \int dt_{pr} \int dt_{pu} \times W_{pr}(\omega_{pr},t_{pr}) W_{pu}(\omega_{pu},t_{pu}) \tilde{S}(t_{pr},\omega_{pr},t_{pu},\omega_{pu}). \quad (7)$$

This equation calculates the pump-probe signal intensity by integrating the time-frequency description of the sample response function $\tilde{S}$ over all frequencies and times. In a pump-probe experiment it is common to spectrally resolve the probe pulse after the interaction with the sample in order to observe the dynamics occurring at different probe energies. This corresponds to passing the probe pulse (after interaction with the sample) through one (such as an interference filter or a monochromator) or more (such as the pixels of a spectrometer) narrow-bandpass filters, each with transfer function $F(\omega_{pr}) = f(\omega_{pr} - \omega_{pr0})$ centered at a specific probe frequency ω_{pr0}. The signal then becomes

$$I_{pp}(\omega_{pr0}) = \frac{1}{(2\pi)^2} \int \int d\omega_{pr} dt_{pr} F(\omega_{pr}) W_{pr}(\omega_{pr},t_{pr}) \int d\omega_{pu} \times \int dt_{pu} W_{pu}(\omega_{pu},t_{pu}) \tilde{S}(t_{pr},\omega_{pr},t_{pu},\omega_{pu}). \quad (8)$$

To define the effective temporal resolution in a pump-probe experiment, in the approximation of well-separated pulses, we assume a sample with an instantaneous response function $\tilde{S}(t_{pr},\omega_{pr},t_{pu},\omega_{pu}) = \delta(t_{pu} - t_0)A(\omega_{pu})$, which is frequency modulated by the sample absorption function $A(\omega_{pu})$. It should be noted that we have considered the strictest condition for the experimental temporal resolution retrieval since the pump fields are not time ordered. Equation (6) can then be rewritten as

$$I_{pp}(\omega_{pr0}) = \frac{1}{(2\pi)^2} \int dt_{pr} \int d\omega_{pr} F(\omega_{pr}) W_{pr}(\omega_{pr},t_{pr}) \times \int d\omega_{pu} A(\omega_{pu}) W_{pu}(\omega_{pu},t_0). \quad (9)$$

We now define a *preparation window* $\xi_{pu}(t)$ as the temporal marginal of the pump WS weighted by the sample absorption spectrum:

$$\xi_{pu}(t) = \int A(\omega_{pu}) W_{pu}(\omega_{pu},t)\, d\omega_{pu}. \quad (10)$$

The preparation window describes the effective temporal window over which the pump interacts with the sample. We note that when the sample absorption spectrum is constant throughout the entire pump frequency range $[A(\omega_{pu}) = \text{const}]$, the preparation window $\xi_{pu}(t)$ coincides with the pump intensity profile $|E_{pu}(t)|^2$ (i.e., the temporal marginal of the pump pulse WS); in contrast, an absorption spectrum narrower than or partially overlapping with the pump spectrum will "shape" the preparation window, making it generally shorter than the pump intensity profile.

We further define an *observation window* $\xi_{pr}(t)$ as the temporal marginal of the probe WS weighted by the transfer function of the filter in detection:

$$\xi_{pr}(t) = \int F(\omega_{pr}) W_{pr}(\omega_{pr},t)\, d\omega_{pr}. \quad (11)$$

The observation window describes the effective duration of the interaction between the perturbed sample and the specific probe spectral slice under consideration (i.e., observed by the detection system). For open-band detection $[F(\omega_{pr}) = \text{const}]$ the preparation window $\xi_{pr}(t)$ coincides with the probe intensity profile $|E_{pr}(t)|^2$ (i.e., the temporal marginal of the probe pulse WS).

Using Eqs. (10) and (11) and defining a pump-probe delay $\tau_{pp} = t_{pr} - t_0$, the pump-probe signal can be rewritten as

$$I_{pp}(\tau_{pp}) = \frac{1}{(2\pi)^2} \int dt_{pr} \xi_{pr}(t_{pr}) \xi_{pu}(t_{pr} - \tau_{pp}) \equiv \frac{1}{(2\pi)^2} \xi_{pr} \otimes \xi_{pu}, \quad (12)$$

where $\otimes$ stands for cross-correlation. Equation (12) is the main result of this paper and shows that this function, which, for instantaneous sample response, determines the temporal resolution in pump-probe spectroscopy, is the temporal cross-correlation between the preparation window $\xi_{pu}(t)$ and the observation window $\xi_{pr}(t)$. Equation 18 generalizes the well-known result for TL pulses, with the preparation and observation windows playing the roles of pump and probe intensity profiles, respectively. It should be noted, however, that Eq. (12) intimately depends on the sample absorption and its spectral overlap with the pump WS [see Eq. (10)]: for this reason, it is not a purely *instrumental* response function and is hereafter called the ERF.

C. Roles of the preparation and observation windows

To clarify the role of preparation and observation windows in determining the ERF, let us consider the WS of an optical pulse supporting 6-fs TL and strongly chirped with a pure quadratic spectral phase up to a duration of 100 fs [see Fig. 2(a)]. As previously discussed, its narrow and elongated shape is caused by a shear of the WS of the corresponding TL pulse along the temporal axis. Integration of the WS over the time and frequency axes [see Eqs. (2)] leads to the pulse spectrum and the pulse intensity profile, respectively, shown in Figs. 2(b) and 2(c) as dashed (black) lines. In the following

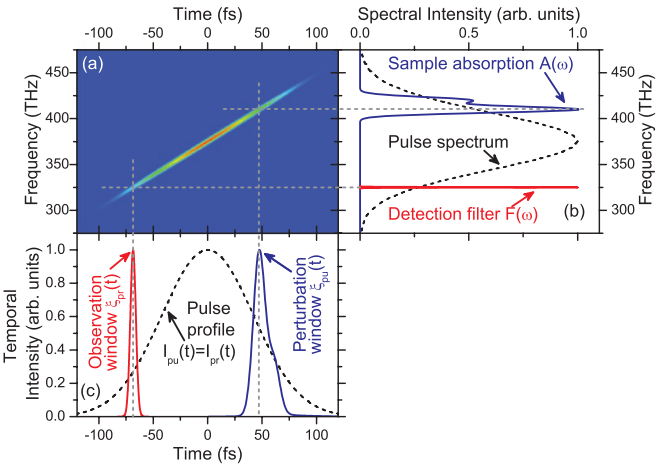

FIG. 2. (Color online) (a) WS of an optical pulse supporting a 6-fs TL duration and strongly chirped, with a pure quadratic phase (GDD = 216 fs^2) up to 100 fs in duration. (b) Pulse spectrum (WS integrated over the time axis), sample absorption spectrum, and detection filter. (c) Pulse temporal profile (WS integrated over the frequency axis) and preparation and observation windows.

this chirped pulse will represent either the pump or the probe pulse.

Let us first consider the case of a chirped pump pulse. Figure 2(b) shows a sample absorption spectrum [solid (blue) line], which overlaps with the pump pulse only in a narrow spectral region. The resulting preparation window $\xi_{\mathrm{pu}}(t)$, calculated using Eq. (10), is shown in Fig. 2(c): its 15-fs FWHM duration is considerably shorter than the 100-fs duration of the chirped pump pulse. Therefore the use of a broadband pump pulse, even in the presence of a strong uncompensated frequency chirp, still allows a considerable gain in the time resolution of the experiment. It should be noted that the use of a TL pump pulse whose spectrum matches the absorption line of the sample would reduce the temporal resolution by 1 order of magnitude. Note that the preparation window can be much shorter than the spectrally integrated pump pulse width even with a broad sample absorption band, when there is a partial spectral overlap between the pump and the sample absorption spectra (see Sec. III).

Let us now turn to the observation window. In Fig. 2(b) we display the filter function $F(\omega_{\mathrm{pr}})$ representing the spectral response of a typical narrow-band detection system with an ≈0.9-THz spectral width (corresponding to ≈2 nm in this wavelength range): compared to the broad probe pulse spectrum, it can be approximated by a δ function $\delta(\omega_{\mathrm{pr}}-\omega_0)$ centered at ω_0. Therefore, using Eq. (11) the observation window can be expressed as $\xi_{\mathrm{pr}}(t) \cong W_{\mathrm{pr}}(\omega_0,t)$. In particular, for a probe pulse with a purely quadratic spectral phase, as in Fig. 2, the WS can be expressed by Eq. (4). Therefore, any spectral slice (with a narrow bandwidth) of W_{CHIRPED} is a rigid temporal translation of the corresponding TL slice, and the temporal resolution is rigorously preserved [see the resulting preparation window with ≈6-fs FWHM plotted in Fig. 2(c)], although the time 0 is shifted for each probe wavelength. This is not strictly true when higher-order dispersion terms are included, yet the additional broadening is limited (see Fig. 4). It is important to note that the ERF depends on the bandwidth of

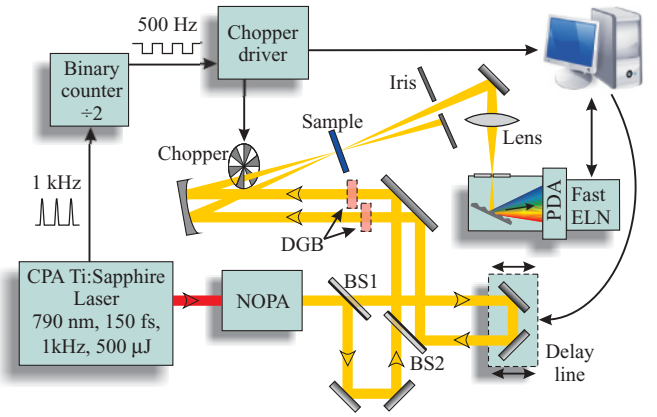

FIG. 3. (Color online) Schematic drawing of the developed experimental setup. CPA Ti:sapphire, chirped-pulse amplified Ti:sapphire laser system; NOPA, noncollinear optical parametric amplifier; BS1 and BS2, beam splitters; DGB, dispersive glass blocks; PDA, photodiode array; fast ELN, fast electronics.

the filter function $F(\omega_{\mathrm{pr}})$ and varies across the probe frequency range. Our results agree with the commonly used procedure for chirped WLC probe pulses, which consists of applying a frequency-dependent temporal shift to the transient absorption spectra. However, it is important to note that the WLC has a bandwidth which is sufficient to support a TL duration of ≈4 fs, and this can be the duration of the observation window even

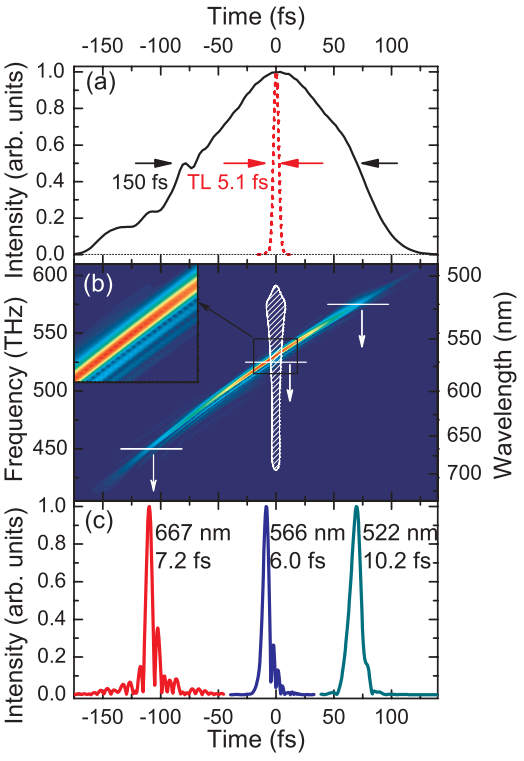

FIG. 4. (Color online) (a) Wavelength-integrated pulse profiles. (b) WS of the TL (hatched area) and chirped pulses (obtained upon propagation of the TL pulse inside a 2.5-mm-thick sapphire plate; color contour) together with a closeup of the latter pulse. (c) Temporal profiles obtained by spectrally slicing the chirped pulse at selected wavelengths.

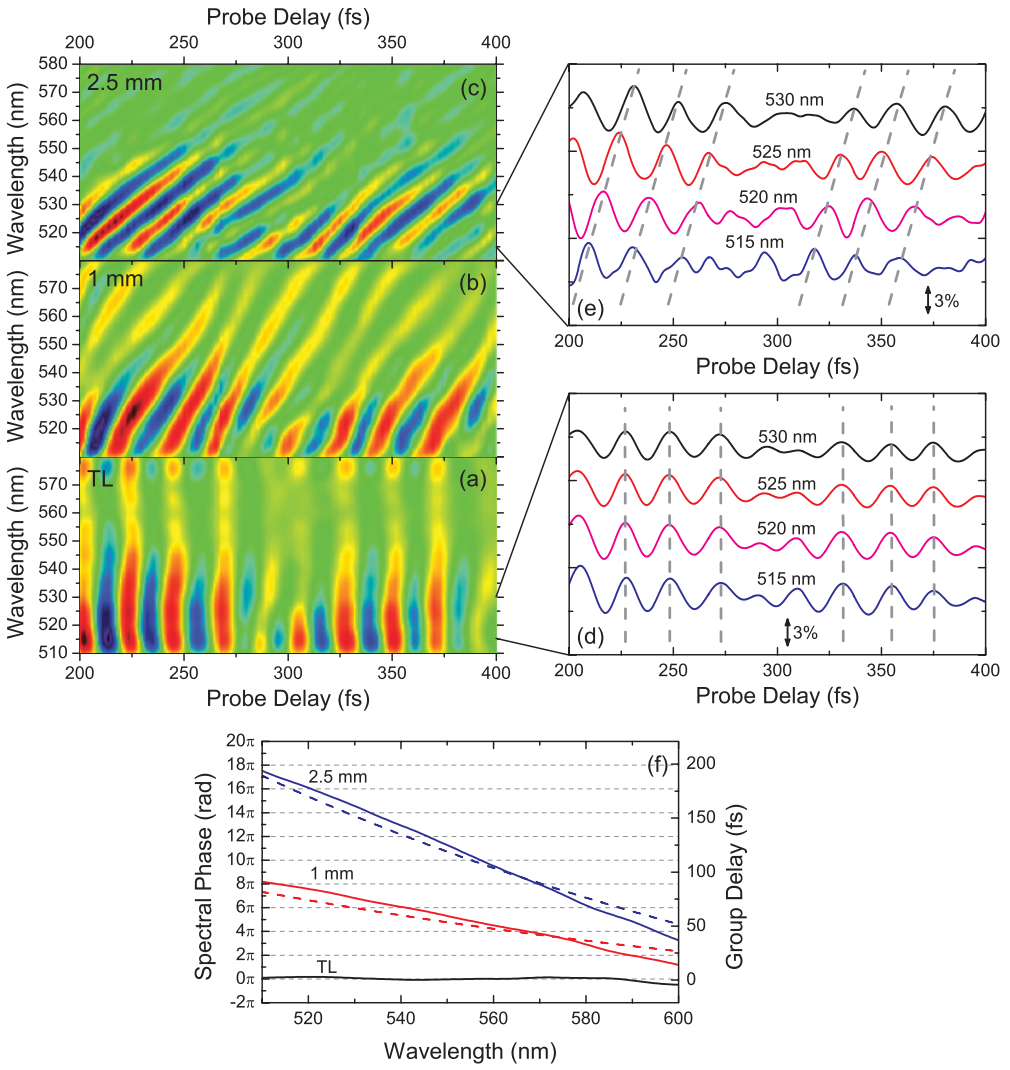

FIG. 5. (Color online) (a–c) $\Delta T/T$ plots as a function of probe wavelength and delay in PPV-C60 for different values of probe pulse chirp. (d, e) Pump-probe dynamics for (d) transform-limited (TL) and (e) strongly chirped probe pulses. (f) Solid lines: spectral phase of the Fourier transform at 1585 cm^{-1} frequency (C = C stretching) and corresponding GD for the TL pulse and the chirped ones. Dashed lines: simulated GDs introduced by the sapphire plates.

with uncompressed WLC, if a suitable narrow-band filter is used in detection. To exploit such a high resolution, of course, a correspondingly short preparation window is required, by using either a short pump pulse or a narrow spectral overlap with the sample absorption.

III. EXPERIMENT

A. Methods

The experimental setup is sketched in Fig. 3. It starts with a regeneratively amplified Ti:sapphire laser delivering 150-fs pulses at 790 nm at 500-μJ energy and a 1-kHz repetition rate (Clark-MXR model CPA-1). An ≈100-μJ fraction of this light is used to pump a home-built noncollinear optical parametric amplifier (NOPA) which generates ultrabroadband pulses with microjoule-level energy and spectra spanning the 500- to 700 nm wavelength range [22,23]. The pulses are compressed down to nearly TL ≈ 5 fs duration with chirped mirrors and sent to a degenerate pump-probe setup. After the sample the probe beam is selected by an iris and sent to an OMA with fast electronics, allowing single-shot recording of the probe spectrum at the full 1-kHz repetition rate [24]. Two-dimensional differential transmission $\Delta T/T(\lambda_{pr}, \tau_{pp})$ maps as a function of the probe wavelength λ_{pr} and delay τ_{pp} are acquired in a few minutes with a high sensitivity.

The NOPA pulses have been fully characterized in amplitude and phase using the frequency-resolved optical gating (FROG) technique [25]. The compressed pulses have a nearly TL ≈ 5 fs FWHM duration [see dashed (red) line in Fig. 4(a)]; their calculated WS is plotted in Fig. 4(b) as the hatched area. To generate chirped pulses, sapphire plates with different thicknesses are inserted along the laser path before the sample, as shown in Fig. 3. For example, using a 2.5-mm-thick plate, the pulse is lengthened to a spectrally integrated FWHM duration of 150 fs [solid (black) line in Fig. 4(a)]. The corresponding WS is shown in Fig. 4(b) as a color contour. The temporal profiles obtained by spectrally slicing the chirped

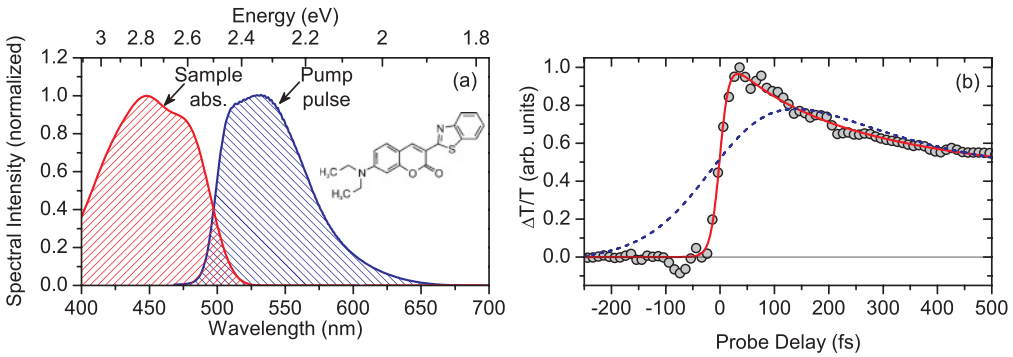

FIG. 6. (Color online) (a) Coumarin 6 absorption spectrum and pump pulse spectrum. Inset: Coumarin 6 chemical structure. (b) Measured $\Delta T/T$ dynamics at a 540-nm probe wavelength (filled circles) together with the calculated best fits using the 40-fs ERF [solid (red) line], compared with the fit obtained considering pump/probe pulses with a 150-fs duration [dashed (blue) line].

pulse WS at selected probe frequencies (observation windows) are plotted in Fig. 4(c): due to the presence of third- and higher-order terms in the spectral phase introduced by the sapphire plate, they are slightly longer than the TL pulse but still much shorter than the spectrally integrated pulse profile.

B. Results and discussion

The first experiment focused solely on the observation window, using a TL pump pulse and a chirped probe pulse. We studied thin films consisting of blends of polyphenylenevinylene (PPV) and fullerene [26]. The pump resonantly excites the first singlet transition of PPV; a rapid electron transfer to the fullerene then occurs, with an ≈50-fs time constant, quenching the singlet exciton population in PPV [27]. The 5-fs pump generates coherent vibrational wave packets in the PPV moiety in both the excited- and the ground-state potential energy surfaces. However, the excited-state vibrational coherence is quenched by the rapid electron transfer process, so that the periodic modulations are solely due to ground-state vibrational coherence induced via impulsive stimulated Raman scattering [28]. Figure 5(a) shows the oscillatory component of the $\Delta T/T$ signal measured using TL probe pulses. We observe a complex vibrational pattern due to the beating of two modes at frequencies $\nu_a \cong 1320\ \mathrm{cm}^{-1}$ (period $T_a \cong 25$ fs) and $\nu_b \cong 1585\ \mathrm{cm}^{-1}$ ($T_b \cong 21$ fs), corresponding to the single and double carbon-bond stretching, respectively [29]. The phase of the oscillations is almost flat across the entire probe spectrum [see also Fig. 5(d)], as expected for a ground-state vibrational mode probed to the red of the steady-state absorption peak [30].

Figures 5(b) and 5(c) show results for probe pulses with a strong positive chirp induced by sapphire plates inserted along their path before the sample, with 1-mm [Fig. 5(b)] and 2.5-mm [Fig. 5(c)] thicknesses, corresponding to GDDs $D \approx 100$ and 250 fs^2, respectively; the resulting probe pulse widths (measured by FROG) are 55 and 150 fs (see the WS in Fig. 4). Astonishingly, even with probe pulses that are ≈7 times longer than the oscillation period, the oscillatory pattern is still visible, with no loss of contrast, although it is now strongly bent [note the 2π phase shift occurring in the 15-nm spectral region plotted in Fig. 5(e)]. According to Eq. (11), considering an $F(\omega_{\mathrm{pr}})$ function with an ≈2-nm FWHM determined by the spectral resolution of our OMA, in the case of 150-fs probe pulses the observation window indeed has a FWHM duration in the sub-10-fs range, depending on the probe wavelength. Note that the fringe pattern would be washed out in an open-band detection scheme or, for example, using interference filters with a pass-band of ≈10 nm. Figure 5(f) shows the probe wavelength dependence of the spectral phase φ for the 1585 cm^{-1} mode (solid line), as extracted from the Fourier transform of the oscillatory pattern, and the corresponding group delay (GD) calculated as $\mathrm{GD} = \varphi^* T_b/2\pi$. The results are in very good agreement with the calculated GD introduced by the sapphire windows [dashed lines in Fig. 5(f)]. Incidentally, we note that in these circumstances the experiment represents a way to characterize the spectral phase of the chirped probe pulse [31].

To highlight the role of the preparation window, we performed a second experiment by strongly chirping both pump and probe pulses up to 150-fs duration. In this case the sample is a drop-cast film of coumarin 6 dye. Figure 6(a) shows its chemical structure and its absorption spectrum, which presents a partial overlap with the pump spectrum. Following Eq. (10), the calculated preparation window has an ≈40-fs FWHM duration, which also determines the duration of the ERF [due to the considerably shorter, ≈10-fs, observation window with narrow-band detection; see Eq. (17)]. Pump-probe dynamics at a 540-nm probe wavelength is plotted in Fig. 6(b) as filled circles. The $\Delta T/T$ signal, due to stimulated emission from the first singlet excited state, has a prompt formation and decays within a few picoseconds. The data can be well fitted using a simple rate equation model convoluted with the ERF [solid (red) line in Fig. 6(b)]. For comparison, we also plot, as the dashed (blue) line, the best fit obtained using the instrumental response function with the 150-fs FWHM pump/probe intensity profiles, which shows a much longer rise time with respect to the experimentally observed one.

IV. CONCLUSIONS

In this paper we have performed a rigorous analysis of broadband pump-probe experiments and provided a precise definition of the effective temporal resolution in the case of chirped pulses. We have demonstrated that, even in the presence of a strong frequency chirp, one can recover the temporal resolution of the nearly TL pulse, provided

that (i) the probe pulse is detected through a narrow-band filter, such as a monochromator or an OMA; (ii) the sample absorption spectrum either is narrow compared to the pulse spectrum or partially overlaps it. We find that for chirped broadband pulses the temporal resolution is not purely instrumental but also depends on the sample absorption spectrum. Our results should help the design of pump-probe spectroscopy setups using chirped broadband pulses. We find that accurate dispersion compensation is not always required and that a broadband chirped pulse provides a significantly improved resolution compared to narrow-band TL pulses with the same spectrally integrated duration. For example, our results could be applied to chirped continua generated by high-order harmonics in the extreme ultraviolet spectral range, where dispersion compensation is challenging and the sample transitions are relatively narrow-band compared to the pump spectrum. The understanding of light-matter interaction with chirped pulses, provided by our study, will facilitate novel observations of very fast dynamical processes.

ACKNOWLEDGMENTS

S.M. was supported by the Chemical Sciences, Geosciences and Biosciences Division, Office of Basic Energy Sciences, Office of Science, US Department of Energy. D.P. acknowledges funding from Politecnico di Milano under the project "Understanding the Architecture of Photosynthetic Light Harvesting by Space and Time Resolved Spectroscopy."

APPENDIX: EXPRESSION OF THE NONLINEAR RESPONSE IN TERMS OF WIGNER SPECTROGRAMS

We start from the pump-probe signal for well-separated pump and probe pulses:

$$I_{\rm pp} = \int_{-\infty}^{\infty} dt'' \int_{-\infty}^{\infty} d\tau'' \int_{-\infty}^{\infty} dt' \int_{-\infty}^{\infty} d\tau' E^*_{\rm pr}(t'') \times E_{\rm pr}(\tau'') S(t'',\tau'',t',\tau') E^*_{\rm pu}(t') E_{\rm pu}(\tau'). \quad \text{(A1)}$$

To describe both pump and probe pulses in terms of their WSs, we perform a change in the variables to $t - \frac{\tau}{2} = t'$ and $t + \frac{\tau}{2} = \tau'$ in Eq. (1a)(a):

$$W\left(\omega, \frac{t'+\tau'}{2}\right) = \int_{-\infty}^{\infty} E^*(t') E(\tau') e^{i\omega(\tau'-t')}\, d\tau'. \quad \text{(A2)}$$

By extracting the terms $E^*(t')e^{-i\omega t'}$ from the integral, we obtain

$$W\left(\omega, \frac{t'+\tau'}{2}\right) = E^*(t')e^{-i\omega t'} \int_{-\infty}^{\infty} E(\tau')e^{i\omega\tau'} d\tau' = E^*(t')e^{-i\omega t'} \tilde{E}(\omega). \quad \text{(A3)}$$

Upon multiplying Eq. (8) by $e^{i\omega(t'-\tau')}$ and integrating over ω, we get

$$\frac{1}{2\pi} \int W\left(\omega, \frac{t'+\tau'}{2}\right) e^{i\omega(t'-\tau')} d\omega = E^*(t')E(\tau'). \quad \text{(A4)}$$

We now substitute Eq. (A4) into Eq. (A1) and express the pump-probe signal as

$$I_{\rm pp} = \frac{1}{(2\pi)^2} \int_{-\infty}^{\infty} dt'' \int_{-\infty}^{\infty} d\tau'' \int_{-\infty}^{\infty} dt' \int_{-\infty}^{\infty} d\tau' \int d\omega_{\rm pr} \times \int d\omega_{\rm pu} W_{\rm pr}\left(\omega_{\rm pr}, \frac{t''+\tau''}{2}\right) e^{i\omega_{\rm pr}(t''-\tau'')} S(t'',\tau'',t',\tau') \times W_{\rm pu}\left(\omega_{\rm pu}, \frac{t'+\tau'}{2}\right) e^{i\omega_{\rm pu}(t'-\tau')}. \quad \text{(A5)}$$

We can change the variables back to get a more compact formula:

$$I_{\rm pp} = \frac{1}{(2\pi)^2} \int d\omega_{\rm pr} \int d\omega_{\rm pu} \int dt_{\rm pr} \int d\tau_{\rm pr} \int dt_{\rm pu} \times \int d\tau_{\rm pu} W_{\rm pr}(\omega_{\rm pr}, t_{\rm pr}) W_{\rm pu}(\omega_{\rm pu}, t_{\rm pu}) \times S\left(t_{\rm pr} - \frac{\tau_{\rm pr}}{2}, t_{\rm pr} + \frac{\tau_{\rm pr}}{2}, t_{\rm pu} - \frac{\tau_{\rm pu}}{2}, t_{\rm pu} + \frac{\tau_{\rm pu}}{2}\right) \times e^{-i\omega_{\rm pr}\tau_{\rm pr}} e^{-i\omega_{\rm pu}\tau_{\rm pu}}. \quad \text{(A6)}$$

Integrals over $\tau_{\rm pu}$ and $\tau_{\rm pr}$ involve only the sample response function S, thus leading to a time-frequency description $\tilde{S}$ of the response, defined by

$$\tilde{S}(t_{\rm pr}, \omega_{\rm pr}, t_{\rm pu}, \omega_{\rm pu}) \equiv \int d\tau_{\rm pr} \int d\tau_{\rm pu} S\left(t_{\rm pr} - \frac{\tau_{\rm pr}}{2}, t_{\rm pr} + \frac{\tau_{\rm pr}}{2}, t_{\rm pu} - \frac{\tau_{\rm pu}}{2}, t_{\rm pu} + \frac{\tau_{\rm pu}}{2}\right) \times e^{-i\omega_{\rm pr}\tau_{\rm pr}} e^{-i\omega_{\rm pu}\tau_{\rm pu}}. \quad \text{(A7)}$$

Inserting Eq. (A7) into Eq. (A6), we finally obtain

$$I_{\rm pp} = \frac{1}{(2\pi)^2} \int d\omega_{\rm pr} \int d\omega_{\rm pu} \int dt_{\rm pr} \int dt_{\rm pu} W_{\rm pr}(\omega_{\rm pr}, t_{\rm pr}) \times W_{\rm pu}(\omega_{\rm pu}, t_{\rm pu}) \tilde{S}(t_{\rm pr}, \omega_{\rm pr}, t_{\rm pu}, \omega_{\rm pu}). \quad \text{(A8)}$$

[1] A. H. Zewail, J. Phys. Chem. A **104**, 5660 (2000).
[2] S. Mukamel, *Principles of Nonlinear Optics and Spectroscopy* (Oxford University Press, New York, 1995).
[3] U. Megerle, I. Pugliesi, C. Schriever, C. F. Sailer, and E. Riedle, Appl. Phys. B **96**, 215 (2009).
[4] F. X. Kärtner, *Few-Cycle Laser Pulse Generation and Its Applications. Topics in Applied Physics, vol. 95* (Springer, New York, 2004).
[5] Z. Vardeny and J. Tauc, Opt. Commun. **39**, 396 (1981).
[6] E. Tokunaga, A. Terasakiy, and T. Kobayashi, J. Opt. Soc. Am. B **13**, 496 (1996).
[7] S. A. Kovalenko, A. L. Dobryakov, J. Ruthmann, and N. P. Ernsting, Phys. Rev. A **59**, 2369 (1999).
[8] I. Pastirk, V. V. Lozovoy, B. I. Grimberg, E. J. Brown, and M. Dantus, J. Phys. Chem. A **103**, 10226 (1999).
[9] D. Polli, M. R. Antognazza, D. Brida, G. Lanzani, G. Cerullo, and S. De Silvestri, Chem. Phys. **350**, 45 (2008).

[10] R. R. Alfano, ed., *The Supercontinuum Laser Source* (Springer, New York, 2006).
[11] C. J. Bardeen, Q. Wang, and C. V. Shank, Phys. Rev. Lett. **75**, 3410 (1995).
[12] C. J. Bardeen, Q. Wang, and C. V. Shank, J. Phys. Chem. A **102**, 2759 (1998).
[13] G. Lanzani, M. Zavelani-Rossi, G. Cerullo, D. Comoretto, and G. Dellepiane, Phys. Rev. B **69**, 134302 (2004).
[14] A. Wand, S. Kallush, O. Shoshanim, O. Bismuth, R. Kosloff, and S. Ruhman, Phys. Chem. Chem. Phys. **12**, 2149 (2010).
[15] T. Witte, T. Hornung, L. Windhorn, D. Proch, R. de Vivie-Riedle, M. Motzkus, and K. L. Kompa, J. Chem. Phys. **118**, 2021 (2003).
[16] C. Ventalon, J. M. Fraser, M. H. Vos, A. Alexandrou, J.-L. Martin, and M. Joffre, Proc. Natl. Acad. Sci. USA **101**, 13216 (2004).
[17] J. Paye, IEEE J. Quantum Electron. **28**, 2262 (1992).
[18] K.-H. Hong, J.-H. Kim, Y. H. Kang, and C. H. Nam, Appl. Phys. B **74**, S231 (2002).
[19] S. Mukamel, C. Ciordas-Ciurdariv, and V. Khidekel, IEEE J. Quantum Electron. **32**, 1278 (1996).
[20] A. T. N. Kumar, F. Rosca, A. Widom, P. M. Champion, J. Chem. Phys. **114**, 701 (2001).
[21] A. T. N. Kumar, F. Rosca, A. Widom, and P. M. Champion, J. Chem. Phys. **114**, 6795 (2001).
[22] C. Manzoni, D. Polli, and G. Cerullo, Rev. Sci. Instrum. **77**, 023103 (2006).
[23] G. Cerullo, C. Manzoni, L. Lüer, and D. Polli, Photochem. Photobiol. Sci. **6**, 135 (2007).
[24] D. Polli, L. Lüer, and G. Cerullo, Rev. Sci. Instrum. **78**, 103108 (2007).
[25] R. Trebino, K. W. DeLong, D. N. Fittinghoff, J. N. Sweetser, M. A. Krumbügel, B. A. Richman, and D. J. Kane, Rev. Sci. Instrum. **68**, 3277 (1997).
[26] N. S. Sariciftci, L. Smilowitz, A. J. Heeger, and F. Wudl, Science **258**, 1474 (1992).
[27] C. J. Brabec, G. Zerza, G. Cerullo, S. De Silvestri, S. Luzzati, J. C. Hummelen, and S. Sariciftci, Chem. Phys. Lett. **340**, 232 (2001).
[28] G. Ashkenazi, U. Banin, A. Bartana, R. Kosloff, and S. Ruhman, Adv. Chem. Phys. **100**, 229 (1997).
[29] G. Lanzani, G. Cerullo, C. Brabec, and N. S. Sariciftci, Phys. Rev. Lett. **90**, 047402 (2003)
[30] A. T. N. Kumar, F. Rosca, A. Widom, and P. M. Champion, J. Chem. Phys. **114**, 701 (2001).
[31] S. Yeremenko, A. Baltuška, F. de Haan, M. S. Pshenichnikov, and D. A. Wiersma, Opt. Lett. **27**, 1171 (2002).